Thermodynamic Control on the Poleward shift of the Extratropical Jet in Climate Change Simulations

Ying Li* and David W. J. Thompson

Department of Atmospheric Science, Colorado State University, Fort Collins, Colorado, USA

Sandrine Bony

Laboratoire de Météorologie Dynamique, IPSL, CNRS, Université Pierre et Marie Curie, Paris, France

Timothy M. Merlis

Department of Atmospheric and Oceanic Sciences, McGill University, Montreal, Quebec, Canada

Corresponding author address: Ying Li, Department of Atmospheric Science, Colorado State University, 3915 W. Laporte Ave. Fort Collins, CO 80521

E-mail: Ying.Li@colostate.edu

ABSTRACT

Extratropical eddy-driven jets are predicted to shift poleward in a warmer climate. Recent studies have suggested that cloud radiative effects (CRE) may enhance the amplitude of such shifts. But there is still considerable uncertainty about the underlying mechanisms whereby CRE govern the jet response to climate change.

This study provides new insight into the role of CRE in the jet response to climate change by exploiting the output from five global warming simulations run with and without atmospheric CRE (ACRE). It is found that the magnitude of the jet shift under climate change is substantially increased in simulations run with ACRE. It is hypothesized that ACRE enhance the jet response to climate change by increasing the atmospheric meridional temperature gradient in the upper troposphere due to the radiative effects of rising high clouds. That is: 1) The tropopause height lifts under climate change due to the thermodynamic constraints placed on clear-sky radiative cooling; 2) The attendant lifting of high clouds lead to enhanced warming beneath the high cloud layer; and 3) Due to the meridional slope of the tropopause, the warming from rising high clouds leads to increases in the upper tropospheric baroclinicity and, in turn, an enhanced jet shift.

The hypothesis is tested in experiments run with an idealized dry GCM, in which the model is perturbed with a thermal forcing that resembles the ACRE response to warming. It is demonstrated that the enhanced jet shifts found in climate change simulations run with ACRE are consistent with the atmospheric response to the radiative warming associated with rising high clouds.

1. Introduction

Climate models predict a robust poleward shift of the extratropical eddy driven jet and its associated storm track in response to increased greenhouse gases, particularly in the Southern Hemisphere (SH; e.g., Hall et al. 1994; Kushner et al. 2001; Yin 2005; Barnes and Polvani 2013; Vallis et al. 2015). Such shifts are thought to arise in response to changes in the meridional and vertical gradients in atmospheric temperature under climate change and their interactions with waves and wave breaking (e.g., Polvani and Kushner 2002; Lorenz and DeWeaver 2007; Chen and Held 2007; Butler et al. 2010; Lorenz 2014; Frierson 2008). However, the magnitude of the jet response to climate change shows considerable spread across Coupled Model Intercomparison Project Phase 5 (CMIP5) models (Taylor et al. 2012; Barnes and Polvani 2013; Voigt and Shaw 2016).

The spread in the jet response to increasing carbon dioxide (CO_2) has been traced back to cloud radiative effects in numerous previous papers (e.g., Ceppi et al. 2012, 2014; Voigt and Shaw 2015, 2016; Ceppi and Hartmann 2016). In fact, recent studies suggest that roughly half of the total jet shift is *caused* by the cloud radiative effects themseleves (Voigt and Shaw 2015, 2016; Ceppi and Hartmann 2016). These studies apply the cloud locking methodology in idealized aquaplanet models to decompose the circulation response to climate change into 1) contributions from cloud changes while holding sea surface temperature (SSTs) or CO_2 fixed, and 2) contributions from SSTs/CO_2 changes while holding the clouds fixed. In locking experiments run with an atmospheric general circulation model (AGCM) coupled to a mixed-layer aquaplanet ocean, Ceppi and Hartmann (2016) argued that the influence of shortwave (SW) cloud radiative effects on SST and surface baroclinicity are central in governing the amplitude of the atmospheric circulation response. Their results support their earlier findings that the inter-model spread in the SW cloud

radiative effects and their attendant effects on SST are responsible for the inter-model spread in the jet response to global warming (Ceppi et al. 2012, 2014).

However, even in the absence of coupling to the SST field and thus in the absence of SW cloud radiative effects at the surface, climate models still produce a range of different circulation responses to prescribed uniform SST warming (e.g., Stevens and Bony 2013; Voigt and Shaw 2016). In this case, the spread is not due to the direct SST response, but to the SST-mediated response to a given SST change (Sherwood et al. 2015). Using a prescribed-SST idealized aquaplanet configuration, Voigt and Shaw (2015) argue that model differences in longwave (LW) cloud radiative changes lead to model differences in jet shifts in two CMIP5 models. Voigt and Shaw (2016) further study the impact of CRE associated with regional cloud changes, and find that 1) the rising of the tropical high-level clouds and 2) the rising and poleward shift of midlatitude high-level clouds contribute roughly equally to the poleward jet shift and are qualitatively robust in the two CMIP5 aquaplanet models that they analyzed.

Despite widespread evidence that cloud radiative feedbacks influence the jet response to climate change, the underlying mechanisms whereby this occurs have not been fully elucidated. In this study, we provide novel insight into the influence of cloud radiative effect on the jet response to climate change by exploiting the model output from the Clouds On-Off Klimate Intercomparison Experiment (COOKIE) simulation (Stevens et al. 2012) using the Atmospheric Model Intercomparison Project (AMIP) configuration, in conjunction with experiments run with an idealized dry GCM. The effects of clouds on changes in surface SW radiation under climate change are excluded in this approach since SSTs are prescribed. Fixing SSTs allows us to focus on the role of changes in atmospheric cloud radiative effects (ACRE) on the circulation as in Voigt and Shaw (2015, 2016), which are dominated by the LW effects. Our hypothesis is that changes in ACRE act to enhance the poleward jet shift under climate change by increasing the atmospheric meridional

temperature gradient in the upper troposphere due to the systematic lifting of high clouds and their attendant ACRE.

The paper is organized as follows: Section 2 describes the details of the COOKIE simulations, the idealized dry GCM experiments, and diagnostic techniques. Section 3 examines the impact of ACRE on the circulation response to global warming in the COOKIE experiments, tests our hypothesis in idealized GCM experiments, and investigates the inter-model spread in the role of ACRE in enhancing the jet shift. Section 4 reviews the key conclusions.

2. Model and Methods

The influence of ACRE on the large-scale atmospheric circulation response to climate change is explored in the COOKIE simulations, which were run under the auspices of the Cloud Feedback Model Intercomparison Project (CFMIP). The COOKIE simulations include two primary types of experiments, both of which are run with an AGCM forced with the same observed monthly SSTs over the period 1979–2008: 1) control simulations that include the full suite of model ACRE ("ACRE-on" experiments); and 2) perturbed simulations in which the model ACRE are turned off in the radiative computation ("ACRE-off" experiments). In our study, we use the following three sets of 30-year long simulations (Stevens et al. 2012):

- "Control_ACREon" and "Control_ACREoff" simulations, in which monthly-mean SSTs are prescribed from observations over the period 1979–2008 (referred to as "amip" and "off-amip", respectively, in Stevens et al. 2012).

- "4K_ACREon" and "4K_ACREoff" simulations, in which SSTs are raised uniformly by 4K relative to their 1979–2008 values (referred to as "amip4K" and "offamip4K", respectively, in Stevens et al. 2012).

- "4×CO_2_ACREon" and "4×CO_2_ACREoff" simulations, in which CO_2 concentrations are quadrupled relative to their pre-industrial values while SSTs are fixed at their 1979–2008 values (referred to as "amip4×CO_2" and "offamip4×CO_2", respectively, in Stevens et al. 2012).

We explore the differences between the following sets of experiments:

1. "4K_ACREon" minus "Control_ACREon". This difference estimates the effects of 4K surface warming on the atmospheric circulation when ACRE are turned *on*.

2. "4K_ACREoff" minus "Control_ACREoff". This difference estimates the effects of 4K surface warming on the atmospheric circulation when ACRE are turned *off*.

3. The difference between 1) and 2). The differences between 1) and 2) are zero if ACRE have *no* effect on the circulation response to surface warming. Thus the differences between 1) and 2) provide an estimate of the role of ACRE on the circulation response to global warming. As discussed in Section 3e, the inferred effects of ACRE on the circulation response can be viewed as summations of two components: 1) a component? due to the effects of ACRE-related heating on the circulation response (the "direct" effect) and 2) a component due to the effects of ACRE-related heating on the climatological mean circulation which, in turn, influence the circulation response to warming (i.e., the circulation response to external forcing is a function of the base-state).

Analogous differences are explored to estimate the response to 4×CO_2 runs in the COOKIE simulations.

We focus on results based on the atmospheric component of the Institut Pierre-Simon Laplace (IPSL) coupled climate model (version IPSL-CM5A-LR; Dufresne et al. 2013), which has vertically resolved cloud radiative heating rates available for the above experiments and has also been

used in earlier studies on the role of ACRE on the general circulation of the atmosphere in the current climate (Fermepin and Bony 2014; Li et al. 2015, 2017). We examine the inter-model spread of the circulation responses to warming in other numerical models available through the COOKIE project (as listed in Li et al. 2017), with the exception of IPSL-CM5B-LR, which has a large bias in the model climatological mean extratropical circulation (e.g., see Hourdin et al. 2013).

We test our hypothesis motivated by COOKIE simulations in Geophysical Fluid Dynamics Laboratory (GFDL) atmospheric dry dynamical core run in the Held and Suarez (1994) framework. The model is forced by Newtonian relaxation to a prescribed zonally symmetric "radiative equilibrium" temperature field, and is damped by linear Rayleigh friction in the planetary boundary layer. The model is run with the same 39 vertical levels as IPSL-CM5A, and at T42 spectral horizontal resolution with a ∇^8 hyperviscosity that damps the smallest scales on a 12 h timescale. It is integrated with a 15-minute time step for 1000 days. The first 200 days are discarded to account for model spin up.

The latitude of the eddy-driven jet is found by 1) calculating the pressure-weighted average of the zonal winds between 850- and 700-hPa (i.e., lower levels are used to capture the barotropic component of the flow); 2) interpolating cubically onto a 0.1° latitude grid around the peak of the zonal flow; and 3) finding the latitude of the maximum wind speed between 20° and 70° latitude at 0.1° interval.

3. Results

a. The jet response to global warming in different forcing scenarios and model configurations

Figure 1a briefly reviews the zonal-mean zonal wind response to $4\times CO_2$ forcing in the coupled ocean-atmosphere version of IPSL-CM5A-LR model. Consistent with previous studies (Hall et al.

1994; Kushner et al. 2001; Yin 2005; Barnes and Polvani 2013; Vallis et al. 2015), increasing CO_2 leads to a robust poleward shift in the midlatitude SH jet and a relatively weak shift in NH jet. Fig. 1a suggests that the IPSL-CM5A-LR model behaves much like the multi-model ensemble means from all 26 CMIP5 models (ref. Fig. 1 in Grise and Polvani 2014).

The total response to $4\times CO_2$ shown in Fig. 1a can be decomposed into two components (e.g. Deser and Phillips 2009; Bony et al. 2013; Grise and Polvani 2014): 1) the component due to the direct atmospheric radiative forcing of CO_2 while holding SSTs fixed (i.e., $4\times CO_2$_ACREon $-$ Control_ACREon; Fig. 1b), and 2) the component due to increasing SSTs while holding CO_2 fixed (i.e., 4K_ACREon $-$ Control_ACREon); Fig. 1c). The results in Figs. 1b and c (and the other five available COOKIE models; not shown) suggest that the poleward shift of the jet is mostly due to the increases in surface temperature and attendant changes in atmospheric temperature, whereas the direct radiative forcing of CO_2 plays a much weaker role (Grise and Polvani 2014).

How different (or similar) would these results be in the absence of ACRE? We answer this question by using the COOKIE experiments to assess the role of ACRE on the circulation response to the direct effects of rising SSTs (Fig. 2) and increasing CO_2 (Fig. 3). The left column of Figure 2 shows the effects of 4K warming on zonal-mean temperature and zonal wind changes when ACRE are *on* (i.e., 4K_ACREon $-$ Control_ACREon; note that Fig. 2a is identical to Fig. 1c), and the middle column of Figure 2 shows the effects of 4K warming on the corresponding changes when ACRE are *off* (i.e., 4K_ACREoff $-$ Control_ACREoff). As discussed in section 2, the differences between the left and middle columns of Fig. 2 can be viewed as the total effects of ACRE on the circulation response to global warming (right column of Fig. 2). Comparing the left and middle columns, the poleward shift of the jet has larger amplitude when ACRE are included in the simulations (Fig. 2c). The results in Fig. 2c support earlier findings that roughly half of the total

jet shift is due to cloud radiative effects (Voigt and Shaw 2015, 2016; Ceppi et al. 2014; Ceppi and Hartmann 2016).

The vertical structures of the zonal-mean temperature responses to 4K warming (Figs. 2d and 2e) are dominated by large warming in the tropical upper troposphere, as expected since the tropics closely follow the moist adiabatic lapse rate. The tropical upper tropospheric warming gives rise to 1) increases in the upper tropospheric meridional temperature gradient and 2) increases in tropical vertical stability, both of which are responsible for the poleward shift of the midlatitude jet (e.g., Lorenz and DeWeaver 2007; Chen and Held 2007; Chen et al. 2007; Frierson 2008; Butler et al. 2010). Note the weak cooling in the high-latitudes near 150 hPa must be dynamically driven (as opposed to radiatively driven) in response to poleward jet shift.

Consistent with the larger amplitude of the poleward shift of the jet in Fig. 2c, the meridional temperature gradient in the upper troposphere between 100–150 hPa is also much larger when ACRE are included in the simulation (Fig. 2f). The inferred influence of ACRE on the response to 4K warming shown in Figs. 2c and f is very similar to the inferred influence of cloud LW radiative forcing in the climate change experiments run in Voigt and Shaw (2016; compare with their Fig. 6i).

Figure 3 shows analogous results for the $4\times CO_2$ simulations (i.e., SSTs are held fixed; note that Fig. 3a is identical to Fig. 1b). The vertical structure of the zonal-mean temperature response to the CO_2 direct effect is characterized by stratospheric cooling, as expected from the increased LW emission due to CO_2 increasing (Fig. 3d). As such, the meridional temperature gradient is enhanced in the upper troposphere, and there is a weak poleward shift of the jet (Fig. 3a). As is the case for increasing SSTs (Fig. 2), the inclusion of ACRE leads to a larger shift in the SH jet (Fig. 3c). However, the effects of ACRE on the jet responses to increasing CO_2 are relatively weak when SSTs are held fixed (compare Figs. 2c and 3c).

In the following, we will focus on understanding the role of ACRE on the zonal-mean eddy-driven jet response in the +4K warming experiments. As noted above, the jet response to 4K warming is associated with an increased atmospheric meridional temperature gradient in the upper troposphere, and this gradient is enhanced when ACRE are turned on. As shown below, the enhancement of the meridional temperature gradient in the upper troposphere by ACRE changes under warming plays a key role in the associated enhancement of the jet shift.

b. Interpretation of the changes in clouds and ACRE in the +4K warming experiment

The most prominent features in the cloud response to $+4K$ warming (Fig. 4a) are increases in cloud fraction above the control high-cloud maximum and decreases in cloud fraction below the control high-cloud maximum, indicating an upward shift in high-level clouds at all latitudes. The upward shift of high-level clouds is expected from the lifting of the tropopause at all latitudes (also see Fig. 5a). That the clouds shift with the tropopause is anticipated on the basis of the thermodynamic constraint placed on the temperature of high clouds in both the tropics, i.e., via the fixed anvil temperature hypothesis (FAT; Hartmann and Larson 2002; Kuang and Hartmann 2007; Zelinka and Hartmann 2010; Popke et al. 2013), and the extratropics (Thompson et al. 2017). The lifting of the tropopause and deepening of the troposphere in response to warming is consistent with previous studies (Santer et al. 2003; Singh and O'Gorman 2012; Vallis et al. 2015). The most prominent features in the ACRE response to $+4K$ warming (Fig. 4b) are increases in ACRE above the control cloud radiative heating maximum, and decreases in ACRE above the control cloud radiative heating minnum. As such, the same basic lifting of high level clouds (Fig. 4a) extends to ACRE (Fig. 4b) across all latitudes.

Figures 5 and 6 explore to what extent the above changes in clouds and ACRE are consistent with an upward shift in the tropopause. The tropopause (panel a) and the pressure of the maximum

cloud fraction (panel b) are both lifted by ∼25 hPa in the tropics and by ∼50 hPa in the extratropics in the "4K_ACREon" (dashed line) simulations as compared to the "Control_ACREon" (solid line). The pressure of the maximum (red) and minimum (blue) ACRE is lifted by ∼50 hPa globally (panel c). The relatively small lift in tropical high clouds may be related to the increased static stability and thus slight increases in cloud temperatures in the tropics (Zelinka and Hartmann 2010).

In order to test whether the spatial pattern of the changes in cloud fraction under warming can be reproduced by a simple vertical shift, we lift the cloud fraction in the "Control_ACREon" run at each latitude and pressure by 25 hPa in the tropics and 50 hPa in the extratropics. Similarly, we also lift ACRE in the "Control_ACREon" run at each latitude and pressure by 50 hPa. Figure 6b shows the results of the calculation. As is apparent in the figure, the patterns of clouds (contours) and ACRE (shading) that result from lifting both fields from their control configurations (Fig. 6b) yields patterns that strongly resemble the actual changes in both fields (Fig. 6a; reproduced from shading in Figs 5a and 5b). The actual cloud fraction changes (Fig. 6a) exhibit slightly smaller positive anomalies and larger negative anomalies than those found in the constructed cloud fraction changes (Fig. 6b). These features likely arise from the net reduction in middle and high level cloud fraction found under global warming scenarios (Zelinka et al. 2013; Bony et al. 2016; Voigt and Shaw 2016).

The changes in cloud radiative effects are physically consistent with the lifting of upper level clouds. Specifically, the lifting leads to anomalous warming due to ACRE beneath the level where the cloud fraction anomalies are positive, and anomalous cooling above that level. Due to the meridional slope of the tropopause, the pattern of ACRE associated with rising high clouds has a pronounced meridional gradient. Therefore, the changes in ACRE under warming leads to enhance

the meridional temperature gradient in the upper tropospheric midlatitudes, which subsequently acts to increase the poleward shift of the jet.

In the next subsection, we will use the idealized dry GCM to test the direct effects of the anomalous ACRE associated with a global lifting of the tropopause on the poleward shift of the jet.

c. The circulation response to ACRE in an idealized dry GCM

To explore the isolated effects of the changes in ACRE associated with surface warming on the poleward shift of the jet, we force an idealized dry GCM with the pattern of ACRE obtained from the comprehensive GCM. As described in section 2, in the control simulation of the idealized dry GCM, the atmospheric temperature is driven by Newtonian relaxation toward the prescribed radiative equilibrium temperature profile from Held and Suarez (1994). In the perturbed simulation, we add a thermal forcing as a diabatic heating in the temperature tendency equation in the idealized dry GCM. The thermal forcing is derived from the change in ACRE found between the control and $+4$K experiments (shading in Figs. 4b, 6a). The differences in the circulation between the long term-means of the perturbed and control simulations of the idealized dry GCM can be considered as the "response" to that particular thermal forcing. A similar approach was exploited by Voigt and Shaw (2016), who used an idealized dry GCM to study the jet response to global and regional CRE.

The top panels in Fig. 7 show the two thermal forcings applied here, and the bottom panels show the responses in the zonal-mean temperature field (shading) and wind field (contours). The forcing in Fig. 7a is reproduced from the shading in Figs. 4b and 6a. The response to the thermal forcing includes (Fig. 7c): 1) warming in the tropical troposphere centered at $\sim$150 hPa, juxtaposed against relatively weak cooling in the lower stratosphere poleward of $\sim 50^{\circ}$, 2) westerly changes

in the zonal flow centered around 55°, juxtaposed against easterly changes centered around 35°, and 3) increase in the tropopause height globally (comparing the dashed and solid contours).

Overall, the structure of the changes in the zonal-mean temperature and zonal wind fields in the idealized dry GCM (Fig. 7c) bear a strong resemblance to the effects of ACRE on the circulation in the 4K AGCM simulations (compare 7c with the right panel of Fig. 2). The most notable exception is that the amplitude of the temperature response is 2–3 times larger in the dry model, which may result from 1) differences in model physics between the full GCM and the dry dynamical core, such as the convective scheme and/or other parameterizations which act to damp the temperature response in the comprehensive GCM, and/or 2) the fact that the heating imposed in the dry dynamical core does not account for any attendant changes in clear-sky radiative cooling driven by changes in atmospheric water vapor, which will tend to oppose the effects of ACRE (Voigt and Shaw 2015; Ceppi and Shepherd 2017). The key result in Fig. 7c is that the pattern of ACRE from the comprehensive GCM yields a poleward shift in the model jet similar to the enhancement of the jet shift found when ACRE are included in the +4K simulations.

We performed a second perturbed simulation forced by the radiative warming component of the ACRE in the upper troposphere in isolation (Fig. 7b). The similarities between the circulation responses between the two perturbed simulations (Figs. 7c and 7d) suggest that the changes in the midlatitude circulation are predominantly driven by the increases in upper-tropospheric cloud radiative effects, and that the decreases play a secondary role.

Similar poleward jet shifts have been found in previous idealized dry GCM forced by 1) imposing tropical upper tropospheric warming (Butler et al. 2010; Sun et al. 2013; Voigt and Shaw 2016), 2) imposing midlatitude upper tropospheric warming (Lorenz and DeWeaver 2007; Voigt and Shaw 2016), and 3) raising the tropopause height (Lorenz and DeWeaver 2007). The results

shown in Fig. 7 provide another robust explantation for the poleward jet shift through the changes in ACRE associated with rising high clouds.

d. The inter-model spread of the SH jet shift in the COOKIE experiments

The enhanced jet shift found in response to warming in the COOKIE simulations when ACRE are turned on is robust across different atmospheric models. Figure 8 summarizes and compares the eddy-driven jet latitude in the SH for each AGCM in the control (points on the solid diagonal line) and +4K simulations (points off the diagonal line) when ACRE are on (panel a) and off (panel b). When ACRE are on (Fig. 8a), the jet position in the +4K simulations are all above the diagonal line, indicating the poleward shift of the SH jet. The poleward shift of the jet is about 2°–2.5° latitude among all five models. When ACRE are off, the poleward shift of the jet is evidently smaller in magnitude in all cases (Fig. 8b). The results suggest that the enhanced poleward shift of the jet when ACRE are turned on is qualitatively robust across all five models, although the amplitude of the effect shows considerable spread.

The results in Fig. 8 are shown for the SH only. Although the cloud radiative effects may have an equatorially symmetric impact on the upper tropospheric temperature gradient (as suggested from Fig. 2c), the sign and amplitude of the impact of ACRE on the zonal-mean NH jet shift show a much wider range of responses across the five models than the impact on the SH jet. The effects of ACRE on the jet shift differ over the North Atlantic and North Pacific in some models (not shown). Hence, in the NH it would be more meaningful and accurate to consider the jet response over the North Atlantic and North Pacific separately. A more detailed analysis of the NH storm track response to ACRE under climate change is deferred to a future study.

e. The "indirect" and "direct" responses to ACRE

The influence of ACRE on the circulation response to climate change can be viewed as comprising two components: 1) The "direct" effect, whereby the inclusion of ACRE in the simulation directly influences the circulation response to global warming and 2) The "indirect" effect, whereby the inclusion of ACRE alters the base state climatology, which in turn influences the circulation response to warming. The "direct" and "indirect" effects can be decomposed in the COOKIE framework as follows:

The climate of the control and global warming states can be denoted as T1 and T2, respectively. The ACRE have three different states: A0 (ACRE are turned off), A1 (ACRE from the control simulation), A2 (ACRE from the 4K simulation). Following this notation, the four COOKIE climate change simulations examined here can be written as:

- $T1A1$ (Control_ACREon)
- $T2A2$ (4K_ACREon)
- $T1A0$ (Control_ACREoff)
- $T2A0$ (4K_ACREoff)

The response of the circulation to 4K surface warming *with* interactive ACRE can be expressed as: $T2A2 - T1A1$. The response includes two components: 1) the change in the base state due to the increase in temperature from $T1$ to $T2$, and 2) the change in the circulation due to the change in ACRE state from $A1$ to $A2$. In order to separate the effects of 1) global warming while holding ACRE fixed from 2) changes in ACRE while holding the base state fixed, the total response

$T2A2 - T1A1$ can be expanded as:

$$T2A2 - T1A1 = \frac{1}{2}[(T2A2 - T1A2) + (T2A1 - T1A1)] + \frac{1}{2}[(T2A2 - T2A1) + (T1A2 - T1A1)], \tag{1}$$

Note that $T1A2$ has the control (no warming) base state with ACRE derived from the 4K climate, and $T2A1$ has the 4K base state with ACRE derived from the control climate. The first bracketed term on the RHS represents the effects of warming on the circulation with ACRE are held to both $A1$ and $A2$ states. The second bracketed term on the RHS represents the effects of the changes in ACRE due to global warming on the circulation where the base states are held to the $T1$ and $T2$ states.

Likewise, the response of the circulation to 4K surface warming *without* interactive ACRE can be expressed as:

$$T2A0 - T1A0. \tag{2}$$

Based on Equations (1) and (2), the differences in the circulation response to surface warming between the interactive and non-interactive ACRE cases [i.e., the (4K_ACREon − Control_ACREon) minus (4K_ACREoff − Control_ACREoff)] results shown in the right column of Figs. 2 and 3) can be decomposed into two contributions:

- $\frac{1}{2}[(T2A2 - T2A1) + (T1A2 - T1A1)]$

  As mentioned above, this term represents the effects of the changes in ACRE due to global warming on the circulation where the base states are held to the $T1$ and $T2$ climatologies. Thus, it estimates the differences in the circulation response to global warming due to the "direct" effect of the changes in ACRE.

- $\frac{1}{2}[(T2A2 - T1A2) + (T2A1 - T1A1)] - (T2A0 - T1A0)$

  This term estimates the "indirect" effect of ACRE on the circulation response to global warm-

ing that arises from the effects of ACRE on the climatological mean circulation. These differences arise from the fact that 1) simulation run with ACRE ($A1$ and $A2$) and without ACRE ($A0$) have very different climatological-mean circulations in the both troposphere and stratosphere, even though surface temperatures are unchanged (e.g., Li et al. 2015, 2017; Watt-Meyer and Frierson 2017; Lipat et al. 2017), and 2) the circulation response to global warming is sensitive to the climatological-mean state on which the surface warming are applied (Barnes and Hartmann 2010; Kidston and Gerber 2010; Barnes and Polvani 2013; Simpson and Polvani 2016).

The differences in the circulation response to surface warming between simulations run with and without interactive ACRE (as shown in the right panel of Figs. 2 and 3) include both the "direct" and "indirect" responses outlined above. The COOKIE archive provides $T1A1$, $T2A2$, $T1A0$, $T2A0$. Quantifying the "direct" and "indirect" effects would require the additional locking experiments $T2A1$ and $T1A2$.

Hence, the COOKIE framework does not provide the experiments necessary to distinguish between the two effects. Nevertheless, the idealized dry GCM used in the previous subsection can provide some insights into which effect is dominant. To explore the relative roles of the "direct" and "indirect" effects, we run the following experiments.

First we run the three simulations forced with different ACRE forcing ($A0$, $A1$ and $A2$) on the base climatology in control Held-Suarez state ($T1$):

- $T1A0$ is forced with the Held-Suarez base state ($T1$) and no ACRE forcing ($A0$) (Fig. 9a).

- $T1A1$ is forced with the Held-Suarez base state ($T1$) and the forcing due to ACRE in the control simulation ($A1$) published in Figure 4c of Li et al. (2015)(Fig. 9d).

- $T1A2$ is forced with the Held-Suarez base state ($T1$) and the forcing due to ACRE in the 4K simulation ($A2$) (Fig. 9g). Note that the forcing A2 is equal to the sum of A1 and the heating shown here in Fig. 4b.

The climatological-mean zonal flow for these simulations is shown in the left column of Fig. 9 (Figs. 9a, d and g).

We then run three simulations forced with same above ACRE forcings ($A0$, $A1$ and $A2$), but on top of the base climatology derived from the global warming state ($T2$). The global-warming state is defined as the HS climatology forced with the tropical heating used in Butler et al. (2010, see their Fig. 2a), which mimics the meridional structure of the global warming response in the free atmosphere. The results are shown in the middle column of Fig. 9:

- $T2A0$ is run with the tropical heating superposed on the basic state given by the $T1A0$ simulation (Fig. 9b)

- $T2A1$ is run with the tropical heating superposed on the basic state given by the $T1A1$ simulation (Fig. 9e)

- $T2A2$ is run with the tropical heating superposed on the basic state given by the $T1A2$ simulation (Fig. 9h)

The differences $[T2A0 - T1A0]$, $[T2A1 - T1A1]$ and $[T2A2 - T1A2]$ are shown in the right column of Fig. 9, and show the effects of tropical heating on the circulation when it is applied to the $T1A0$, $T1A1$ and $T1A2$ climatologies, respectively (Figs. 9c, f, i). The term $\frac{1}{2}[(T2A2 - T1A2) + (T2A1 - T1A1)] - (T2A0 - T1A0)$ is shown in Fig. 10b, and is analogous to the "indirect" effect of ACRE on the circulation response to climate change. It indicates effects of the changes in the base state due to the inclusion of ACRE on the response.

The terms $[T1A2 - T1A1]$ and $[T2A2 - T2A1]$ are shown in the bottom row, and indicate the effect of the changes in ACRE from A1 to A2 on the circulation when it is applied to the $T1A1$ and $T2A1$ climatologies, respectively (Figs. 9j, k). The average $\frac{1}{2}[(T1A2 - T1A1) + (T2A2 - T2A1)]$ is shown in Fig. 10a, and corresponds to the "direct" effect of ACRE on the circulation response.

The relative importance of the "indirect" and "direct" effects of ACRE on the circulation response to climate change - as estimated by the simulations run with the idealized dry GCM - can be inferred by comparing Figures 10a and 10b. The results suggest that the inclusion of ACRE in climate change simulations acts to 1) enhance the warming of the tropical troposphere due to the "direct" radiative effects of the changes in ACRE; and 2) enhance the poleward shift of the jet due to both the "direct" radiative effects of the changes in ACRE and the "indirect" effects of ACRE on the base-state climatology.

The simulations run with the idealized dry GCM highlight the nonlinear nature of the jet response to climate change. They also highlight the importance of considering the effects of ACRE on both the base state and the net heating in climate change simulations. However, they are not directly comparable to the COOKIE simulations for several reasons, notably 1) the dry model "ACRE" are imposed as a thermal forcing and are not coupled to the circulation, 2) the dry model "climate change forcing" is given as a simple tropical heating profile, and 3) the meridional shift of the circulation in dry dynamical models is sensitive not only to the base-state climatology but also the meridional scale of the tropical thermal forcing (Tandon et al. 2013; Sun et al. 2013). In fact, we expect that the "true indirect" effect in the COOKIE simulations is much smaller than that estimated from the dry model simulations, since the changes in the base-state climatology due to the inclusion of ACRE in the COOKIE IPSL-CM5A simulations (i.e., as shown in Figs. 5a and 5b in Li et al. 2015) are much smaller than those estimated by the inclusion of ACRE in the idealized dry GCM (i.e., the differences between $T1A1$ and $T1A0$ in Fig. 9d and 9a here; result not shown).

As noted earlier, additional locking experiments are required to quantify the direct and indirectly of the ACRE more accurately.

4. Concluding remarks

In this study, we examined the role of atmospheric cloud radiative effects (ACRE) on the circulation response to climate change. To do so, we explored the differences in the circulation response to climate change in simulations run with and without ACRE in the COOKIE model intercomparison. We also used experiments run with an idealized dry GCM to explore the circulation response to ACRE related thermal forcings. The key results are as follows:

- The magnitude of the poleward jet shift found in response to global warming of 4K is substantially increased in simulations run with ACRE (Figs. 2c, Fig. 8), consistent with earlier findings that roughly half of the total jet shift is due to cloud radiative effects (Voigt and Shaw 2015, 2016; Ceppi and Hartmann 2016).

- The enhanced poleward jet shift due to the inclusion of ACRE appears to derive primarily from the influence of ACRE on the upper tropospheric meridional temperature gradient. Our hypothesis is as follows: 1) Surface warming leads to rising high clouds globally due to the thermodynamic constraint placed on the temperature of the tropopause in both the tropics (Hartmann and Larson 2002) and extratropics (Thompson et al. 2017). In turn, rising high clouds lead to enhanced ACRE in the upper troposphere, and due to the meridional slope of the tropopause, increases in the baroclinicity and a poleward shift of the jet.

- Experiments run with an idealized dry GCM simulations confirm that radiative warming due to ACRE associated with rising high clouds plays a significant role in increasing the meridional temperature gradient in the upper troposphere and enhancing the poleward shift of the

jet (Figs. 7c,d). They also suggest that the influence of ACRE on upper tropospheric temperatures in climate change simulations is dominated by 1) the effects of ACRE on the net heating in the upper troposphere (i.e., the "direct" effect of ACRE) rather than 2) the effects of ACRE on the climatological-mean circulation upon which the heating is imposed (i.e., the "indirect" effect of ACRE).

The poleward shift of the jet in climate change simulations is clearly enhanced when ACRE are included in the simulation (Fig. 8). However, there is considerable inter-model spread in the impact of ACRE on the poleward jet shift from one model to the next. The spread could be due to 1) intermodel variations in the response of the upper tropospheric meridional temperature gradient to changes in ACRE under surface warming (i.e., the "direct" effect of ACRE), 2) intermodel variations in the response of climatological-mean circulation to ACRE, which in turn induce the differences in the circulation response to surface warming (i.e., the "indirect" effect of ACRE), and/or 3) intermodel variations in the amplitude of the ACRE response to surface warming. It is not possible to quantify 1) and 2) in simulations provided in the COOKIE archive, but they could be studied in more detail with additional locking experiments. It is difficult to verify 3) due to the lack of vertically resolved ACRE made available from the COOKIE or CMIP5 archives (Taylor et al. 2012), but this possibly could be addressed in the future when COOKIE-like experiments are available in CMIP6 (Webb et al. 2017).

The key novel finding in our study is the inferred importance of rising high clouds in governing the enhanced jet shift in climate change simulations run with ACRE. As shown in previous studies, the altitude of high clouds is strongly constrained by water vapor radiative cooling rates - and thus the Clausius-Clapeyron relation - not only in the tropics (Hartmann and Larson 2002) but in the extratropics as well (Thompson et al. 2017). As highlighted in Figs. 5–6, lifting the latitude-height

structure of high clouds and ACRE across the globe closely approximates the spatial pattern of the changes in cloud fraction and ACRE in the upper troposphere under global warming. When the resulting pattern of ACRE is applied as a heating in an idealized GCM, it leads to 1) robust increases in the upper-tropospheric temperature gradient and 2) poleward shifts in the extratropical jet. The influence of ACRE on the jet shift may thus be viewed as an additional "robust" response of the circulation to the thermodynamic constraints placed on water vapor concentrations by the Clausius–Clapeyron relationship.

Acknowledgment. Y.L. is funded by NSF Climate and Large-ScaleDynamics (AGS-1547003) and NASA JPL (1439268). D.W.J.T. is funded by NSF Climate and Large-Scale Dynamics (AGS-1343080 and AGS-1547003). S.B. is funded by the European Research Council (ERC Grant 694768). T.M.M. is funded by Natural Science and Engineering Research Council (NSERC) Grant RGPIN-2014-05416 and acknowledges a Compute Canada allocation.

References

Barnes, E. A., and D. L. Hartmann, 2010: Dynamical feedbacks and the persistence of the NAO. *J. Atmos. Sci.*, **67**, 851–865.

Barnes, E. A., and L. M. Polvani, 2013: Response of the midlatitude jets and of their variability to increased greenhouse gases in the CMIP5 model. *J. Climate*, **26**, 7117–7135.

Bony, S., G. Bellon, D. Klocke, S. Sherwood, S. Fermepin, and S. Denvil, 2013: Robust direct effect of carbon dioxide on tropical circulation and regional precipitation. *Nat. Geosci.*, **6**, 447–451.

Bony, S., B. Stevens, D. Coppin, T. Becker, K. A. Reed, A. Voigt, and B. Medeiros, 2016: Thermodynamic control of anvil cloud amount. *Proc. Natl. Acad. Sci.*, **113**, 8927–8932.

Butler, A. H., D. Thompson, and R. Heikes, 2010: The steady-state atmospheric circulation response to climate change-like thermal forcings in a simple general circulation model. *J. Climate*, **23**, 3474–3496.

Ceppi, P., and D. L. Hartmann, 2016: Clouds and the atmospheric circulation response to warming. *J. Climate*, **29**, 783–799, doi:10.1002/2014GL060043.

Ceppi, P., Y.-T. Hwang, D. M. W. Frierson, and D. L. Hartmann, 2012: Southern Hemisphere jet latitude biases in CMIP5 models linked to shortwave cloud forcing. *Geophys. Res. Lett.*, **39**, L19 708, doi:10.1029/2012GL053115.

Ceppi, P., and T. G. Shepherd, 2017: Contributions of Climate Feedbacks to Changes in Atmospheric Circulation. *J. Climate*, **30**, 9097–9118, doi:10.1175/JCLI-D-17-0189.1.

Ceppi, P., M. D. Zelinka, and D. L. Hartmann, 2014: The response of the Southern Hemispheric eddy-driven jet to future changes in shortwave radiation in CMIP5. *Geophys. Res. Lett.*, **41**, 3244–3250, doi:10.1002/2014GL060043.

Chen, G., and I. M. Held, 2007: Phase speed spectra and the recent poleward shift of Southern Hemisphere surface westerlies. *Geophys. Res. Lett.*, **34**, L21 805, doi:10.1029/2007GL031200.

Chen, G., J. Lu, and D. Frierson, 2007: Phase speed spectra and the latitude of surface westerlies: Interannual variability and global warming trend. *J. Climate*, **21**, 5942–5959.

Deser, C., and A. S. Phillips, 2009: Atmospheric circulation trends, 19502000: The relative roles of sea surface temperature forcing and direct atmospheric radiative forcing. *J. Climate*, **22**, 396–413.

Dufresne, J.-L., and Coauthors, 2013: Climate change projections using the IPSL-CM5 earth system model: From CMIP3 to CMIP5. *Climate Dyn.*, **40**, 2123–2165, doi:10.1007/s00382-012-1636-1.

Fermepin, S., and S. Bony, 2014: Influence of low-cloud radiative effects on tropical circulation and precipitation. *J. Adv. Model. Earth Syst*, **06**, doi:10.1002/2013MS000288.

Frierson, D., 2008: Midlatitude static stability in simple and comprehensive general circulation models. *J. Atmos. Sci.*, **65**, 1049–1062.

Grise, K. M., and L. M. Polvani, 2014: Southern Hemisphere clouddynamics biases in CMIP5 models and their implications for climate projections. *J. Climate*, **27**, 6074–6092, doi:10.1175/JCLI-D-14-00113.1.

Hall, N. M. J., B. J. Hoskins, P. J. Valdes, and C. A. Senior, 1994: Storm tracks in a high-resolution GCM with doubled carbon dioxide. *Quart. J. Roy. Meteor. Soc.*, **120**, 1209–1230.

Hartmann, D. L., and K. Larson, 2002: An important constraint on tropical cloud - climate feedback. *Geophys. Res. Lett.*, **29**, 1951, doi:10.1029/2002GL015835.

Held, I. M., and M. J. Suarez, 1994: A proposal for the intercomparison of the dynamical cores of atmospheric general circulation models. *Bull. Amer. Meteor. Soc.*, **75**, 1825–1830.

Hourdin, F., and Coauthors, 2013: LMDZ5B: The atmospheric component of the IPSL climate model with revisited parameterizations for clouds and convection. *Climate Dyn.*, **40**, 2193–2222.

Kidston, J., and E. P. Gerber, 2010: Intermodel variability of the poleward shift of the austral jet stream in the CMIP3 integrations linked to biases in 20th century climatology. *Geophys. Res. Lett.*, **37**, L09 708, doi:10.1029/2010GL042873.

Kuang, Z., and D. L. Hartmann, 2007: Testing the fixed anvil temperature hypothesis in a Cloud-Resolving Model. *J. Climate*, **20**, 2051–2057.

Kushner, P. J., I. M. Held, and T. L. Delworth, 2001: Southern hemisphere atmospheric circulation response to global warming. *J. Climate*, **14**, 2238–2249.

Li, Y., D. W. J. Thompson, and S. Bony, 2015: The influence of atmospheric cloud radiative effects on the large-scale atmospheric circulation. *J. Climate*, **28**, 7263–7278, doi: 10.1175/JCLI-D-14-00825.1.

Li, Y., D. W. J. Thompson, and Y. Huang, 2017: The influence of atmospheric cloud radiative effects on the large-scale stratospheric circulation. *J. Climate*, **30**, 5621–5635, doi:10.1175/JCLI-D-16-0643.1.

Lipat, B. R., G. Tselioudis, K. M.Grise, and L. M. Polvani, 2017: CMIP5 models'shortwave cloudradiative response and climatesensitivity linked to the clima-tological Hadley cell extent. *Geophys. Res. Lett.*, **44**, 5739–5748, doi:10.1002/2017GL073151.

Lorenz, D. J., 2014: Understanding midlatitude jet variability and change using Rossby wave chromatography: Poleward-shifted jets in response to external forcing. *J. Atmos. Sci.*, **71**, 2370–2389, doi:10.1175/JAS-D-13-0200.1.

Lorenz, D. J., and E. T. DeWeaver, 2007: Tropopause height and zonal wind response to global warming in the IPCC scenario integrations. *J. Geophys. Res.*, **112**, D10 119, doi: 10.1029/2006JD008087.

Polvani, L. M., and P. Kushner, 2002: Tropospheric response to stratospheric perturbations in a relatively simple general circulation model. *Geophys. Res. Lett.*, **29**, 1114, doi:10.1029/2001GL014284.

548 Popke, D., B. Stevens, and A. Voigt, 2013: Climate and climate change in a radiative-
549 convective equilibrium version of ECHAM6. *J. Adv. Model. Earth Syst*, **5**, 1–14, doi:10.1029/
550 2012MS000191.

551 Santer, B. D., and Coauthors, 2003: Contributions of anthropogenic and natural forcing to recent
552 tropopause height changes. *Science*, **301**, 479–483.

553 Sherwood, S. C., S. Bony, O. Boucher, C. Bretherton, P. M. Forster, J. M. Gregory, and B. Stevens,
554 2015: Adjustments in the Forcing-Feedback Framework for Understanding Climate Change.
555 *Bull. Amer. Meteor. Soc.*, **96**, 217–228.

556 Simpson, I. R., and L. M. Polvani, 2016: Revisiting the relationship between jet position, forced
557 response, and annular mode variability in the southern midlatitudes. *Geophys. Res. Lett.*, **43**,
558 2896–2903.

559 Singh, M., and P. O'Gorman, 2012: Upward shift of the atmospheric general circulation under
560 global warming: Theory and simulations. *J. Climate*, **25**, 8259–8276.

561 Stevens, B., and S. Bony, 2013: What are climate models missing? *Science*, **340**, 1053–1054.

562 Stevens, B., S. Bony, and M. Webb, 2012: Clouds on-off klimate intercomparison experiment
563 (COOKIE). Tech. rep. [Available online at http://www.euclipse.eu/downloads/Cookie.pdf.].

564 Sun, L., G. Chen, and J. Lu, 2013: Sensitivities and mechanisms of the zonal mean atmo-
565 spheric circulation response to tropical warming. *J. Climate*, **70**, 2487–2504, doi:10.1175/
566 JAS-D-12-0298.1.

567 Tandon, N. F., E. P. Gerber, A. H. Sobel, and L. M. Polvani, 2013: Understanding Hadley cell
568 expansion versus contraction: Insights from simplified models and implications for recent ob-
569 servations. *J. Climate*, **26**, 4304–4321, doi:10.1175/JCLI-D-12-00598.1.

570 Taylor, K. E., R. J. Stouffer, and G. a. Meehl, 2012: An overview of CMIP5 and the experiment
571 design. *Bull. Amer. Meteor. Soc.*, **93**, 485–498, doi:10.1175/BAMS-D-11-00094.1.

572 Thompson, D. W. J., S. Bony, and Y. Li, 2017: Thermodynamic constraint on the depth of the
573 global tropospheric circulation. *Proc. Natl. Acad. Sci.*, **114**, 8181–8186.

574 Vallis, G., P. Zurita-Gotor, C. Cairns, and J. Kidston, 2015: Response of the large-scale structure
575 of the atmosphere to global warming. *Quart. J. Roy. Meteor. Soc.*, **141**, 1479–1501.

576 Voigt, A., and T. A. Shaw, 2015: Radiative changes of clouds and water vapor shape circulation
577 response to global warming. *Nat. Geosci.*, **8**, 102106, doi:10.1038/ngeo2345.

578 Voigt, A., and T. A. Shaw, 2016: Impact of regional atmospheric cloud radiative changes on shifts
579 of the extratropical jet stream in response to global warming. *J. Climate*, **29**, 8399–8421, doi:
580 10.1175/JCLI-D-16-0140.1.

581 Watt-Meyer, O., and D. M. W. Frierson, 2017: Local and emote impacts of atmospheric cloud
582 radiative effects onto the eddy-driven jet. *GRL*, **44**, 10 036–10 044.

583 Webb, M. J., and Coauthors, 2017: The Cloud Feedback Model Intercomparison Project (CFMIP)
584 contribution to CMIP6. *Geosci. Model Dev. Discuss*, doi:10.5194/gmd-10-359-2017.

585 Yin, J. H., 2005: A consistent poleward shift of the storm tracks in simulations of 21st century
586 climate. *Geophys. Res. Lett.*, **32**, L18 701, doi:10.1029/2005GL023684.

587 Zelinka, M., S. Klein, K. Taylor, T. Andrews, M. Webb, J. Gregory, and P. Forster, 2013: Contri-
588 butions of different cloud types to feedbacks and rapid adjustments in CMIP5. *J. Climate*, **26**,
589 5007–5027, doi:10.1175/JCLI-D-12-00555.1.

590 Zelinka, M. D., and D. L. Hartmann, 2010: Why is longwave cloud feedback positive? *J. Geophys.*
591 *Res.*, **115**, D16 117, doi:10.1029/2010JD013817.

LIST OF FIGURES

Fig. 1. The response in zonal-mean zonal wind (shading) to climate change in the IPSL-CM5A-LR model. a) the difference between the abrupt $4\times CO_2$ (average over the last 50 years) and preindustrial control run (all available years); b) contribution from direct atmospheric CO_2 forcing only ($4\times CO_2$_ACREon–Control_ACREon), and (c) contribution from SST-mediated effect only (4K_ACREon–Control_ACREon). Gray contours denote the corresponding climatology in each control cases (contour interval: 10 m s^{-1}). In each panel, zonal-mean zonal wind response larger than 9.5 m s^{-1} are indicated as white contours at 1 m s^{-1} intervals. 31

Fig. 2. Circulation response (shading) to 4K warming when ACRE are on (left column) and off (middle column), and the differences between left and middle columns. Panel a is reproduced from Fig. 1c. Top panels are for the zonal-mean zonal wind, and bottom panels are for the zonal-mean temperature. Zonal-mean zonal wind response larger than 9.5 m s^{-1} are indicated as white contours at 1 m s^{-1} intervals in panels a-b. Zonal-mean zonal wind response larger than 5.1 m s^{-1} are indicated as white contours at 0.6 m s^{-1} intervals in panels c. Gray contours denote the corresponding climatology (contour interval of zonal-mean zonal wind: 10 m s^{-1}; contour interval of zonal-mean temperature: 10 K) in the Control_ACREon (left column) and Control_ACREoff (middle column). 32

Fig. 3. Same as Fig. 2, but for the circulation response (shading) to $4\times CO_2$ when ACRE are on (left column) and off (middle column), and the differences between left and middle columns. Panel a is reproduced from Fig. 1b. The top panels are for the zonal-mean zonal wind, and the bottom panels are for the zonal-mean temperature. Gray contours denote the corresponding climatology in the Control_ACREon (left) and Control_ACREoff (middle column). . . . 33

Fig. 4. The response in cloud (left) and cloud radiative effects (ACRE; right) to 4K warming when ACRE are on. Gray contours denote the corresponding climatology (contour interval of cloud fraction : 4%; contour interval of cloud radiative heating rate: 0.15 K day^{-1}) in the Control_ACREon. 34

Fig. 5. The pressure of the tropopause (left), maximum in cloud fraction (middle), and maximum/minimum in ACRE (right) as a function of latitude. The solid lines indicates results from the Control_ACREon. The dashed lines indicate results from 4K_ACREon. Red (blue) lines on the right panel indicate results for the pressure of the maximum warming (cooling) in the ACRE. Results are smoothed with a latitudinal running mean filter for display purposes. 35

Fig. 6. (Left) The simulated differences in clouds (contours; contour interval: 1%) and ACRE (shading) between 4K_ACREon and Control_ACREon. (Right) The constructed differences in clouds (contours) and cloud radiative heating rates (shading) between Control_ACREon centered at (ϕ, $p+\delta p$) and Control_ACREon centered at (ϕ, p). δp is 25 hPa the tropics and 50 hPa in the extratropics for cloud field, and δp is 50 hPa at all latitudes. Values below 700 hPa are masked out. 36

Fig. 7. (a) Thermal forcing added in the idealized dry GCM obtained from differences in ACRE between 4K_ACREon and Control_ACREon (reproduced from the shading in Fig. 4a). (b) As in a), but for only the radiative warming component of the ACRE. (c–d) The response in zonal-mean temperature (shading) and zonal wind (contours; contour interval: 2.5 m s^{-1}) to the thermal forcings in a and b, respectively. Solid and dashed lines are the tropopause height in the control and perturbed simulations, respectively. 37

Fig. 8. Mean jet positions in the control and +4K simulations when ACRE are on (left) and off (right). The jet positions in the control simulations are on the solid diagonal line; the jet positions in the +4K experiments are off the diagonal line and indicated by values on the ordinate axis. Arrows connect mean jet positions between the two simulations. Different colored circles denote the different models available from the COOKIE archive. 38

Fig. 9. (a-b, d-e, g-h) Zonal-mean temperature (shading) and zonal-mean zonal wind (contours; contour interval: 5 m s^{-1}) for the simulations forced with six different combinations of thermal forcing (T1, T2) and and ACRE forcing (A0, A1, A2) as described in section e. (c,f,i,j,k) Changes in temperature (shading) and zonal-mean zonal wind (contours; contour interval: 2.5 m s^{-1}). (c) is the difference between (b) and (a), (f) is the difference between (e) and (d), (i) is the difference between (h) and (g), (j) is the difference between (g) and (d), (k) is the difference between (h) and (e). 39

Fig. 10. Zonal-mean temperature (shading) and zonal-mean zonal wind (contours; contour interval: 2.5 m s^{-1}) for the direct and indirect of the ACRE on circulation response in dry model. See section 3e for details. 40

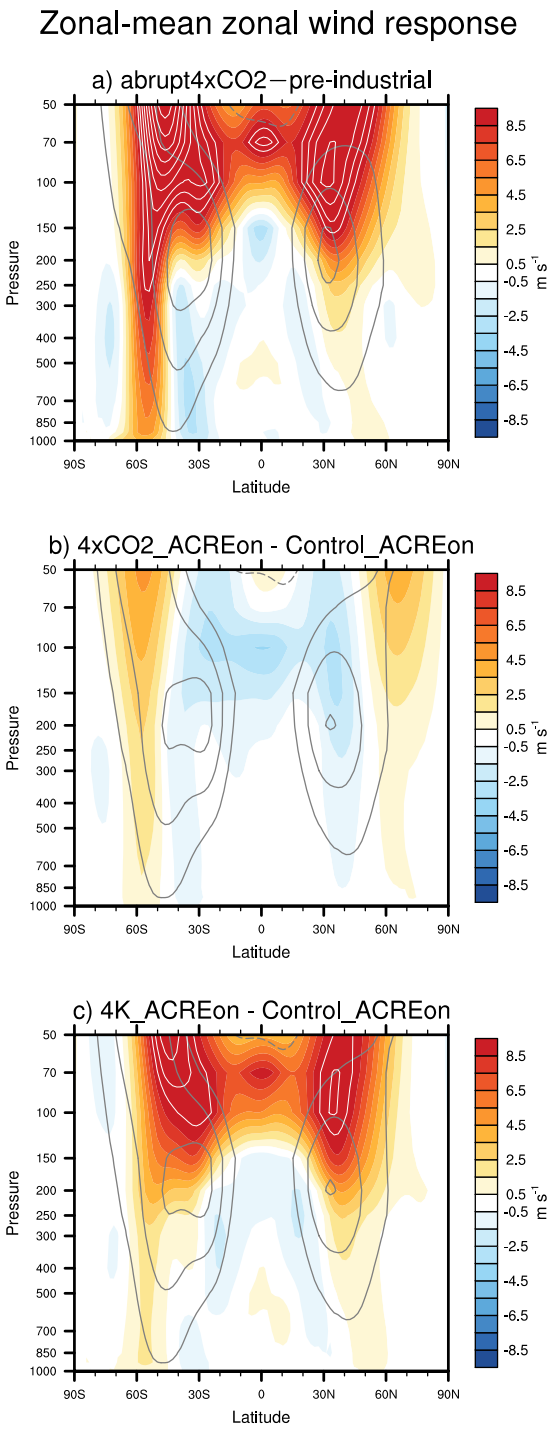

652 FIG. 1. The response in zonal-mean zonal wind (shading) to climate change in the IPSL-CM5A-LR model. a)
653 the difference between the abrupt $4\times CO_2$ (average over the last 50 years) and preindustrial control run (all avail-
654 able years); b) contribution from direct atmospheric CO_2 forcing only ($4\times CO_2$_ACREon–Control_ACREon),
655 and (c) contribution from SST-mediated effect only (4K_ACREon–Control_ACREon). Gray contours denote the
656 corresponding climatology in each control cases (contour interval: 10 m s^{-1}). In each panel, zonal-mean zonal
657 wind response larger than 9.5 m s^{-1} are indicated as white contours at 1 m s^{-1} intervals.

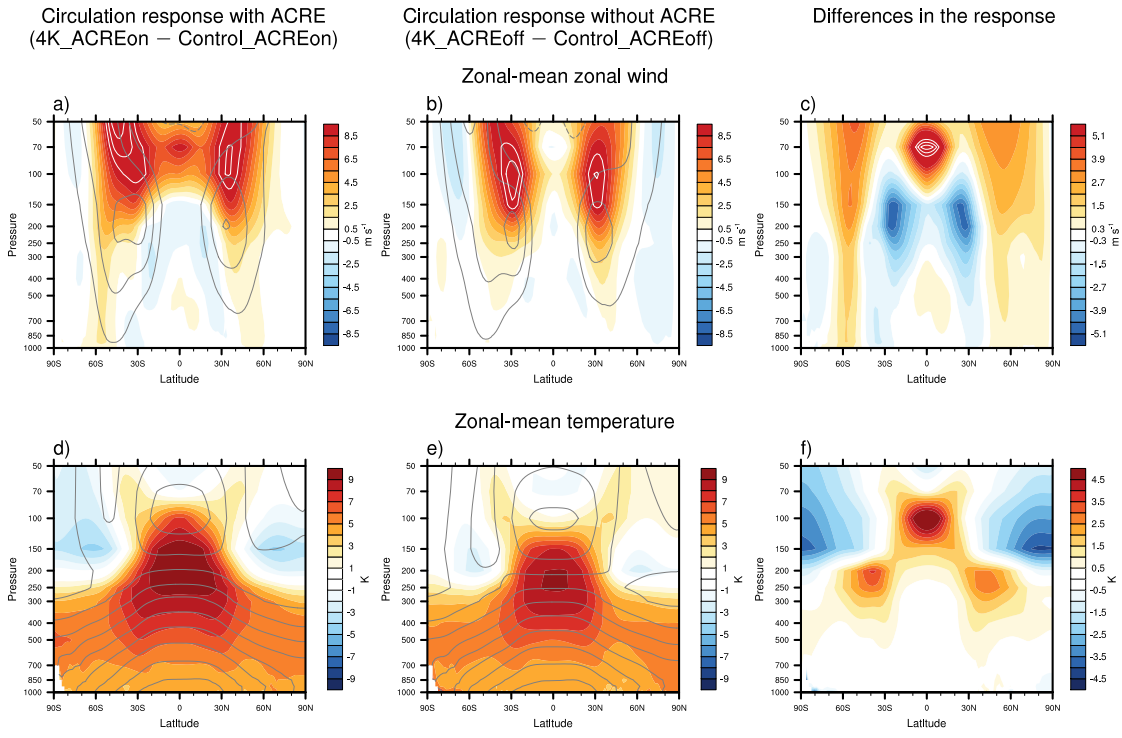

658 FIG. 2. Circulation response (shading) to 4K warming when ACRE are on (left column) and off (middle
659 column), and the differences between left and middle columns. Panel a is reproduced from Fig. 1c. Top panels
660 are for the zonal-mean zonal wind, and bottom panels are for the zonal-mean temperature. Zonal-mean zonal
661 wind response larger than 9.5 m s^{-1} are indicated as white contours at 1 m s^{-1} intervals in panels a-b. Zonal-
662 mean zonal wind response larger than 5.7 m s^{-1} are indicated as white contours at 0.6 m s^{-1} intervals in panels
663 c. Gray contours denote the corresponding climatology (contour interval of zonal-mean zonal wind: 10 m s^{-1};
664 contour interval of zonal-mean temperature: 10 K) in the Control_ACREon (left column) and Control_ACREoff
665 (middle column).

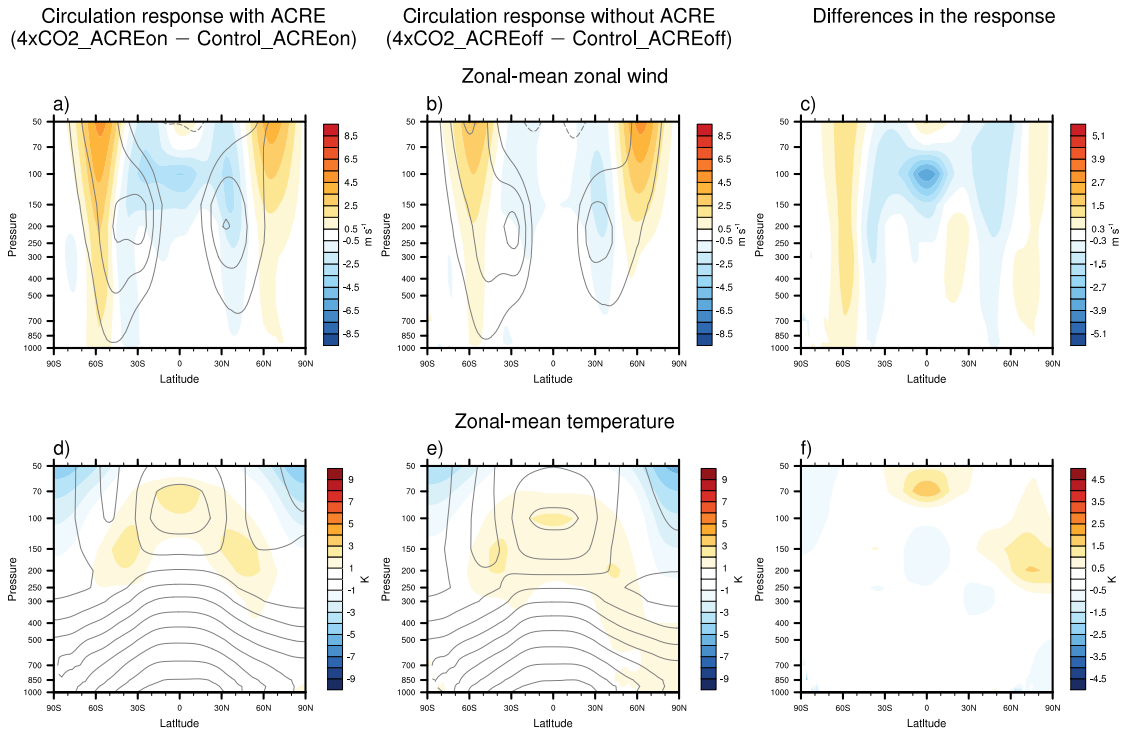

666 FIG. 3. Same as Fig. 2, but for the circulation response (shading) to $4\times CO_2$ when ACRE are on (left column)
667 and off (middle column), and the differences between left and middle columns. Panel a is reproduced from
668 Fig. 1b. The top panels are for the zonal-mean zonal wind, and the bottom panels are for the zonal-mean temper-
669 ature. Gray contours denote the corresponding climatology in the Control_ACREon (left) and Control_ACREoff
670 (middle column).

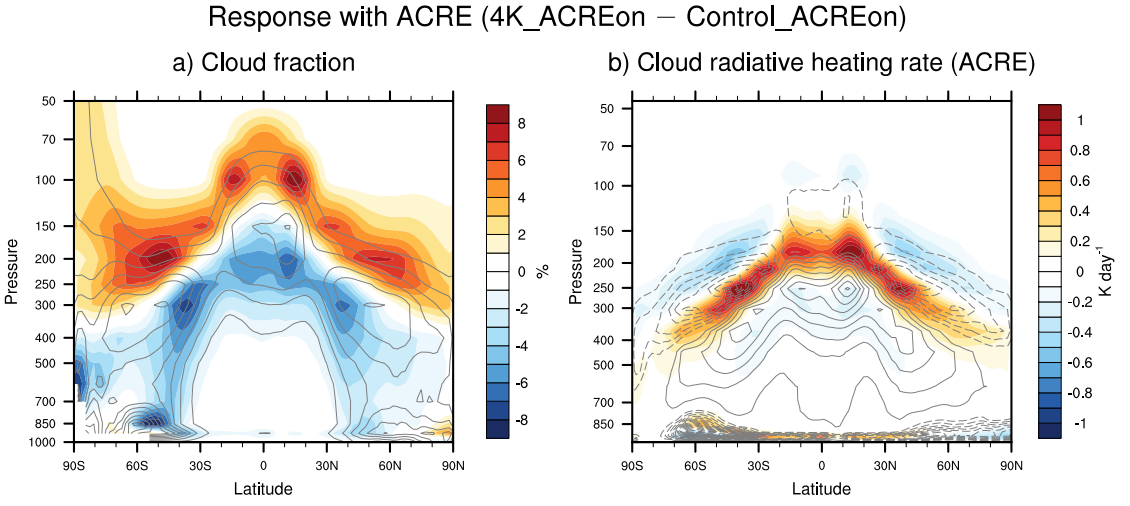

671 FIG. 4. The response in cloud (left) and cloud radiative effects (ACRE; right) to 4K warming when ACRE
672 are on. Gray contours denote the corresponding climatology (contour interval of cloud fraction : 4%; contour
673 interval of cloud radiative heating rate: 0.15 K day^{-1}) in the Control_ACREon.

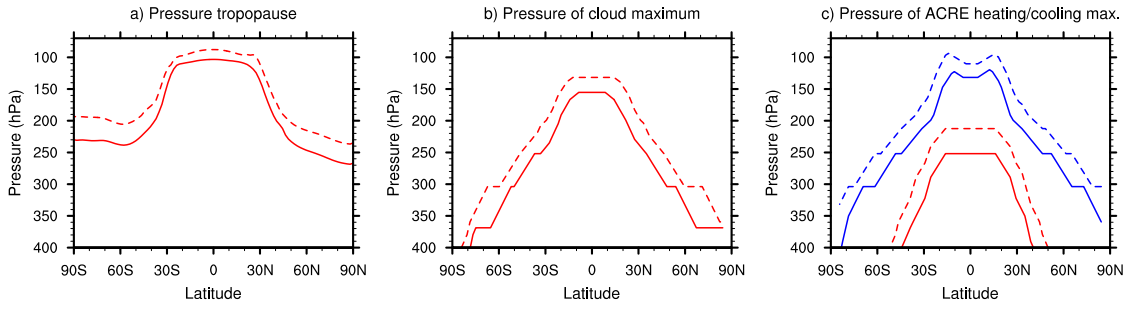

FIG. 5. The pressure of the tropopause (left), maximum in cloud fraction (middle), and maximum/minimum in ACRE (right) as a function of latitude. The solid lines indicates results from the Control_ACREon. The dashed lines indicate results from 4K_ACREon. Red (blue) lines on the right panel indicate results for the pressure of the maximum warming (cooling) in the ACRE. Results are smoothed with a latitudinal running mean filter for display purposes.

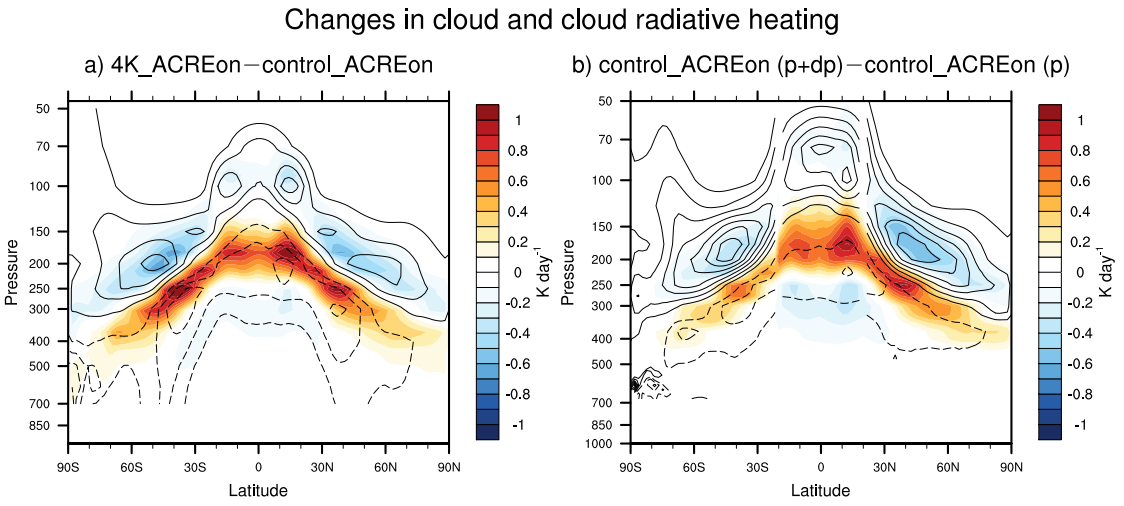

FIG. 6. (Left) The simulated differences in clouds (contours; contour interval: 1%) and ACRE (shading) between 4K_ACREon and Control_ACREon. (Right) The constructed differences in clouds (contours) and cloud radiative heating rates (shading) between Control_ACREon centered at $(\phi,\ p+\delta p)$ and Control_ACREon centered at $(\phi,\ p)$. δp is 25 hPa the tropics and 50 hPa in the extratropics for cloud field, and δp is 50 hPa at all latitudes. Values below 700 hPa are masked out.

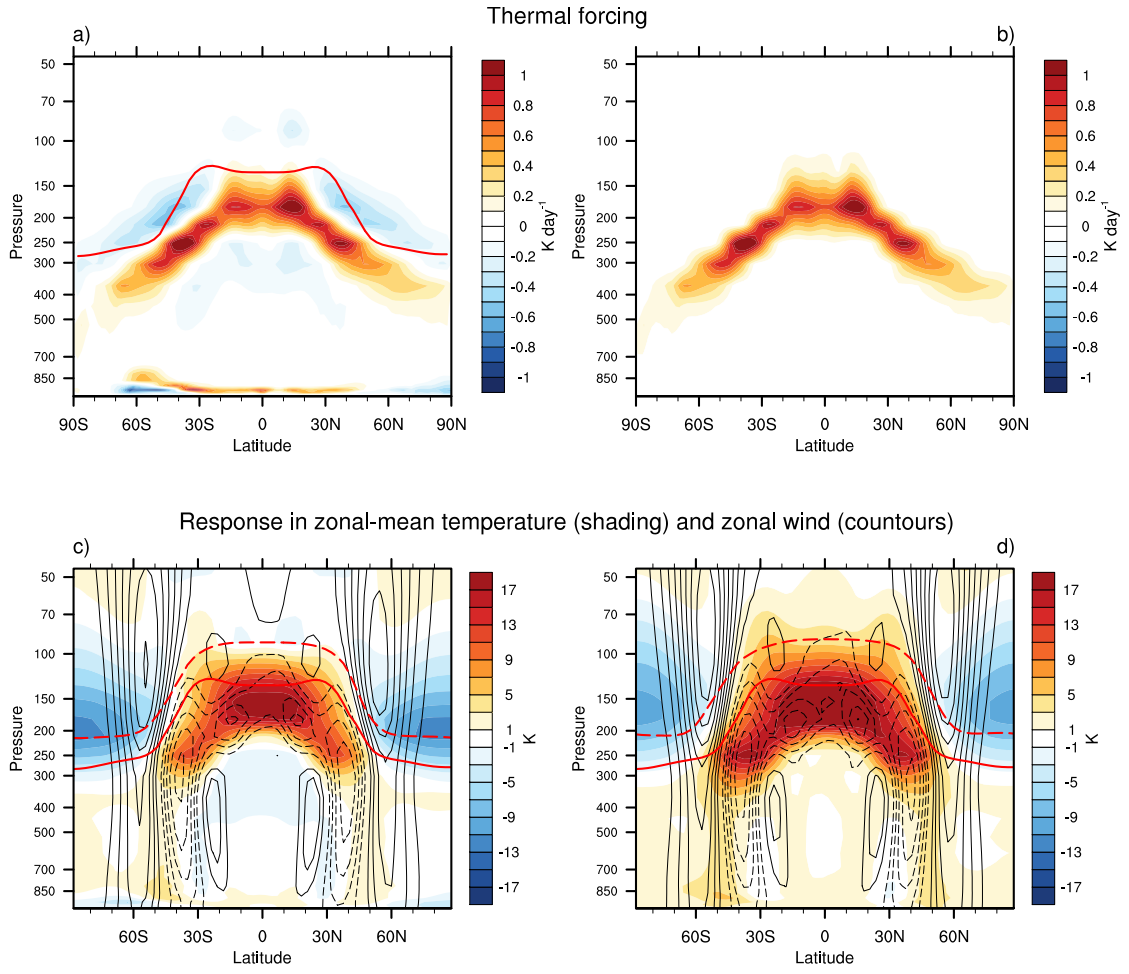

FIG. 7. (a) Thermal forcing added in the idealized dry GCM obtained from differences in ACRE between 4K_ACREon and Control_ACREon (reproduced from the shading in Fig. 4a). (b) As in a), but for only the radiative warming component of the ACRE. (c–d) The response in zonal-mean temperature (shading) and zonal wind (contours; contour interval: 2.5 m s^{-1}) to the thermal forcings in a and b, respectively. Solid and dashed lines are the tropopause height in the control and perturbed simulations, respectively.

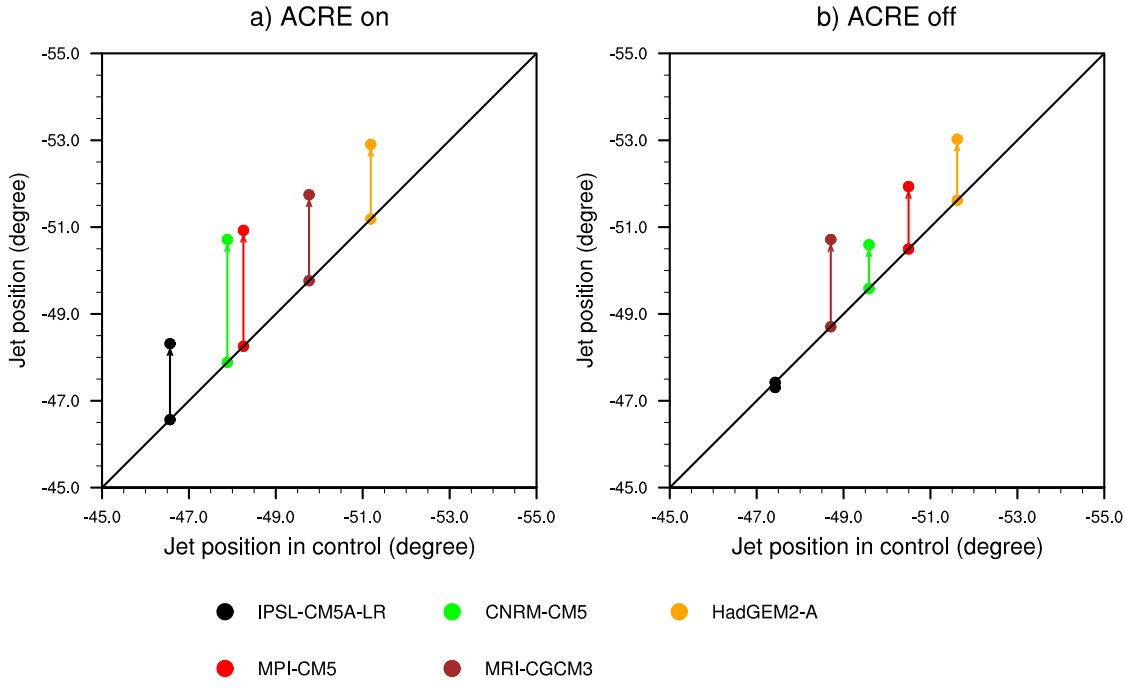

689 FIG. 8. Mean jet positions in the control and +4K simulations when ACRE are on (left) and off (right). The
690 jet positions in the control simulations are on the solid diagonal line; the jet positions in the +4K experiments
691 are off the diagonal line and indicated by values on the ordinate axis. Arrows connect mean jet positions between
692 the two simulations. Different colored circles denote the different models available from the COOKIE archive.

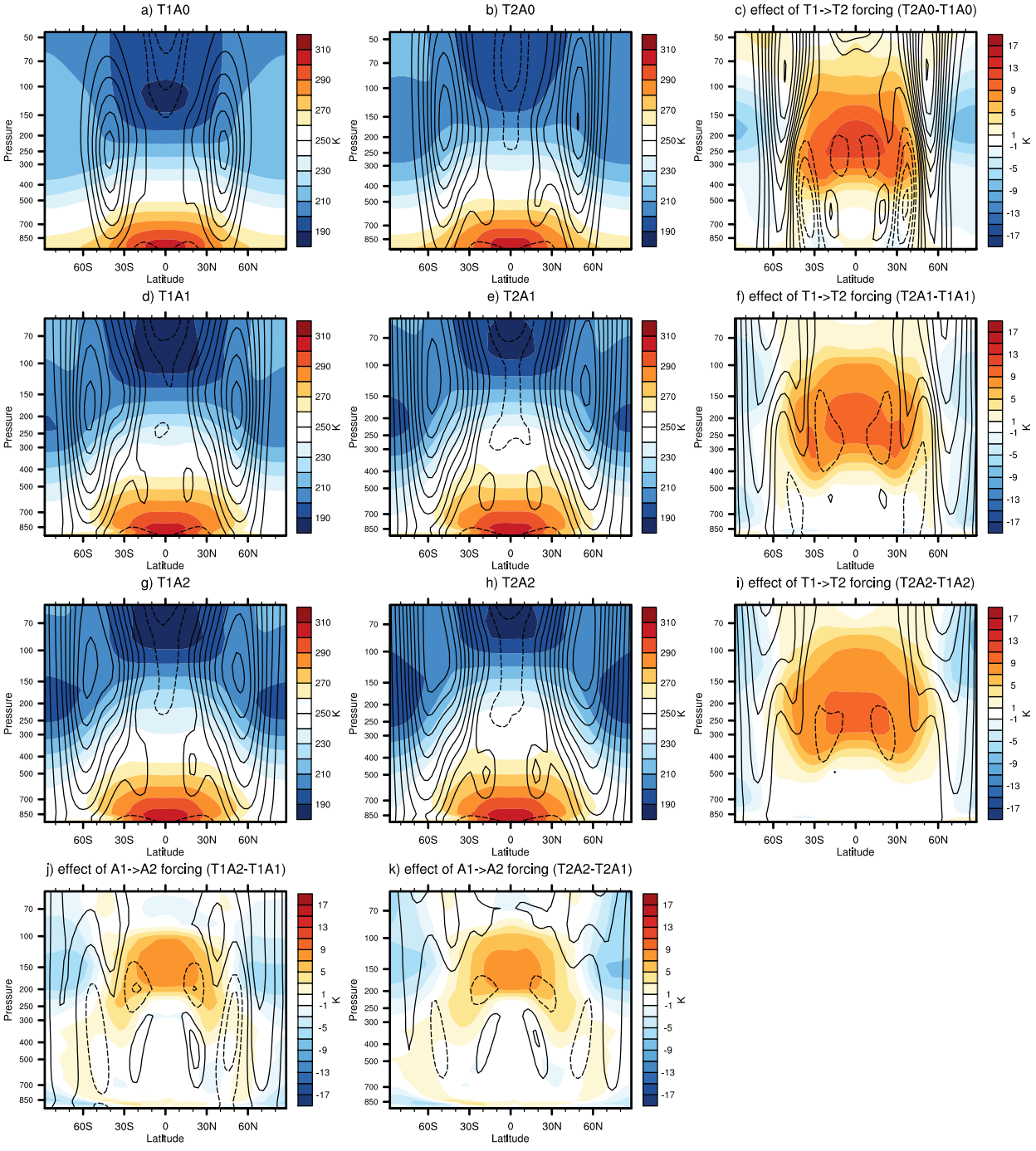

693 FIG. 9. (a-b, d-e, g-h) Zonal-mean temperature (shading) and zonal-mean zonal wind (contours; contour
694 interval: 5 m s^{-1}) for the simulations forced with six different combinations of thermal forcing (T1, T2) and
695 and ACRE forcing (A0, A1, A2) as described in section e. (c,f,i,j,k) Changes in temperature (shading) and
696 zonal-mean zonal wind (contours; contour interval: 2.5 m s^{-1}). (c) is the difference between (b) and (a), (f) is
697 the difference between (e) and (d), (i) is the difference between (h) and (g), (j) is the difference between (g) and
698 (d), (k) is the difference between (h) and (e).

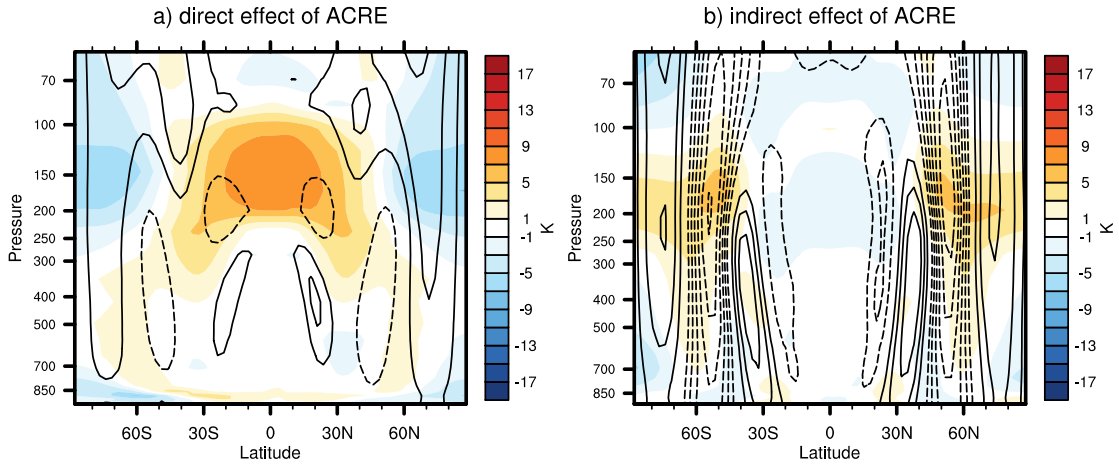

699 FIG. 10. Zonal-mean temperature (shading) and zonal-mean zonal wind (contours; contour interval: 2.5 m
700 s^{-1}) for the direct and indirect of the ACRE on circulation response in dry model. See section 3e for details.